ChemBioChem

Chemistry Europe
European Chemical Societies Publishing
ChemBioChem

RESEARCH ARTICLE OPEN ACCESS

Light-Activated Communication Between Synthetic and Living Cells via Photoresponsive Membranes

Roberto Barbaro[1] | Paola Albanese[1,2,3] | Matilde Colella[4] | Davide Lattarulo[1] | Samrat Saha[2] | Jack L.-Y. Chen[3,5,6] | Fabio Mavelli[1] | Federico Rossi[2] | Emiliano Altamura[1]

[1]Department of Chemistry, University of Bari Aldo Moro, Bari, Italy | [2]Department of Physical Sciences, Earth and Environment, University of Siena, Siena, Italy | [3]Department of Biotechnology, Chemistry and Pharmacy, University of Siena, Siena, Italy | [4]Department of Biosciences, Biotechnology and Environment, University of Bari Aldo Moro, Bari, Italy | [5]School of Science, Auckland University of Technology, Auckland, New Zealand | [6]The MacDiarmid Institute for Advanced Materials and Nanotechnology, Wellington, New Zealand

Correspondence: Emiliano Altamura (emiliano.altamura@uniba.it)

Received: 15 May 2026 | **Revised:** 29 June 2026 | **Accepted:** 2 July 2026

Keywords: biomimetic membranes | cell signaling | cell to cell communication | controlled delivery | photoswitch | rupture of membranes | signal transduction | synthetic cells

ABSTRACT

Synthetic cells (SCs) are programmable biomimetic systems that reproduce selected cellular functions while offering high structural and functional controllability. A particularly attractive feature of SCs is their ability to respond to external stimuli, enabling regulated cargo release and communication with living cells. Here, we report a light-responsive SC platform capable of establishing chemically mediated communication with human cancer cells. Upon light stimulation, the SCs release signaling molecules, such as adenosine triphosphate (ATP) and histamine, that activate intracellular calcium signaling pathways in target cells. These results demonstrate the feasibility of remotely controlled communication between synthetic and living cells and highlight the potential of SCs as bio-hybrid interfaces for precise cellular modulation, therapeutic delivery, artificial organelles, and other biomedical applications.

1 | Introduction

Synthetic cells (SCs) are engineered nano- and micro-structures designed to reproduce selected structural and functional features of living cells. These systems are typically constructed from lipid-based vesicles or polymer-based assemblies (polymersomes) functionalized with synthetic molecules and/or biological building blocks. In contrast to living cells, where thousands of interconnected biochemical reactions occur concurrently, SCs can be assembled using only the minimal set of components required for the desired function. Precise control over system composition, architecture and dynamics, enables the isolation and quantitative investigation of processes otherwise difficult to dissect in natural cellular environments. Owing to this high degree of controllability, SCs have emerged as valuable tools both for fundamental studies and applied biotechnology [1]. In fundamental research, they enable an "understanding-by-building" approach where biological processes are reconstituted in cell-mimetic systems to elucidate their underlying mechanisms [2–5]. In applied contexts, the programmability of SCs has stimulated growing interest in areas such as drug delivery [6], biosensing [7, 8], biocatalysis [9–11], and therapeutic biomimetic systems [12].

In recent years, considerable efforts have been devoted to the development of stimulus-responsive SCs capable of sensing and responding to environmental cues through defined and controllable pathways. Such systems are particularly attractive as smart carriers for therapeutic synthesis and delivery upon stimulation [13, 14], but also as a model platform for investigating minimal cognitive systems [15]. Up to now, SCs have been

Roberto Barbaro and Paola Albanese contributed equally to this work.

engineered to respond to chemical stimuli, including pH [16–19], osmotic shock [18, 20], chemical and enzymatic reactions [21, 22], signal molecules [23–25], as well as to physical triggers such as electromagnetic radiation [26–29], magnetic fields [30], temperature [31], and acoustic waves [32]. These external inputs can induce membrane reorganization or destabilization, leading to controlled transport processes, cargo release, synchronization, or activation of internal biochemical reaction networks. Among the available stimuli, light has emerged as one of the most attractive since it enables noninvasive, reversible, and highly spatiotemporally resolved modulation of biological processes [26]. Photoactive molecular motifs, such as azobenzenes, have been extensively employed due to their reversible *E*–*Z* photoisomerization. Upon UV irradiation, azobenzene undergoes a transition from a thermodynamically stable linear *E* conformation to a metastable bent *Z* configuration, accompanied by substantial variations in molecular geometry and occupied volume. When incorporated into membrane-forming molecules such as amphiphiles [28, 29, 33–36] and phospholipids [37–45], azobenzene isomerization has enabled dynamic optical control over several physicochemical and mechanical properties of the bilayer [37, 38, 46] leading to reversible morphological transformations [28, 29, 34, 42, 47, 48] and permeability modulation [28, 29, 33, 35, 41, 49]. Different azobenzene-based molecules have been shown to efficiently trigger cargo release of the doped membrane through mesh relaxation [28, 29, 49], pore formation [41], or complete vesicle rupture [33, 35], and for this reason, they are attracting considerable interest for next-generation biomedical applications [13, 14].

Indeed, chemical signaling underlies a wide range of cellular functions; thus, the development of SCs capable of on-demand molecular release is highly desirable for enabling communication with living cells and modulating their behavior. Only a few pioneering studies have investigated such scenario. In 2009, Gardner et al. reported the first SC-to-cell signaling study in which a protometabolism, established within the core of SCs, produced metabolites that, once released, triggered quorum-sensing luminescence phenomena in *Vibrio harveyi* bacteria [50]. In other cases, SCs have been engineered to expand the sensing capabilities of model bacteria, transducing a chemical signal that *Escherichia coli* is unable to sense into a signal that can elicit a natural cellular response [8, 51]. In the attempt of improving the programmability and controllability of the communication process with natural cells or with other SCs, liposome-based SCs which operate by gene expression have been lately developed, as reported in [15, 52]. However, these approaches rely on permanently open membrane pores, such as α-hemolysin, for passive cargo release, limiting temporal control, transport selectivity, and internal homeostasis. More recently, Sethi et al. reported an adenosine triphosphate (ATP)-powered strategy for temporally controlled communication between synthetic and living cells [25]. In this system, core–shell microgels act as artificial cells that anchor signaling oligonucleotides through DNA hybridization. An ATP-driven enzymatic reaction network transiently releases the DNA signal into the extracellular medium, enabling its uptake by neighboring mammalian cells, while ATP depletion restores the initial state through signal recapture. Although this approach introduces programmable and reversible communication in response to ATP levels relevant to the tumor microenvironment, the reaction network operates outside the SC and therefore requires all enzymatic and DNA components to be supplied externally. Consequently, the SC mainly functions as a signal storage platform, while the molecular circuitry governing communication remains distributed in the extracellular environment.

In contrast, the implementation of photoresponsive molecules as shell component of SCs, can provide efficient compartmentalization coupled with dynamic and reversible control over the compartment permeability. Transport processes can be activated and deactivated in response to light stimulation and finely regulated with high spatial and temporal precision. Such concept was recently demonstrated by light-triggering SC cargo release for the modulation of gene expression in bacterial populations [8] and in human cells [27]. In these examples, light was exploited to induce chemical transformations of key synthetic-cell building blocks, such as phospholipid membrane crosslinking [8] or photoinduced charge switching in polymersomes [27], thereby activating cargo release and downstream communication with living cells.

Building on these advances, our work explores a complementary communication modality based on the rapid release of small-molecule messengers from biomimetic SCs. Here, giant unilamellar vesicle (GUV)-based SCs were engineered blending 2-oleoyl-1-palmitoyl-*sn*-glycero-3-phosphocholine (POPC) with a photoswitchable azobenzene-based amphiphile. UV-irradiation triggered azobenzene isomerization, affecting SCs stability and ultimately leading to controlled release of encapsulated signaling molecules: ATP and histamine. These chemical messengers were selected as model agonists due to their well-established role in calcium-mediated signaling pathways [53, 54]. Upon optical activation, "sender" SCs release the chemical messengers which are in turn recognized by receptors expressed on neighboring human HeLa cells, triggering intracellular signaling cascades which result in oscillatory cytosolic calcium responses (Figure 1). The present work broadens the toolbox for SC engineering as light-responsive interfaces for the spatiotemporally controlled delivery of molecular messengers to living cells. The release system couples a physical trigger with a stealth-like activation mechanism, remaining functionally silent until irradiation. By enabling rapid release of biologically relevant signaling molecules without the transfer of genetic material, this strategy opens new opportunities for the development of minimally invasive platforms to modulate cellular responses.

2 | Materials and Methods

2.1 | Materials

All reagents and fine chemicals, unless otherwise specified, were purchased from Sigma–Aldrich (Milan, Italy). Phospholipids were purchased from Lipoid GmbH, Steinhausen, Switzerland.

2.2 | Compound 7 Synthetic Route

The targeted photoswitchable amphiphile was readily synthesized following a previously established six-step reaction sequence [28, 55]. In brief, starting from *p*-nitrophenol **1**, an eight-carbon tail was attached to the phenolic –OH by using 1-bromooctane. Then, after reduction of the nitro group to the corresponding

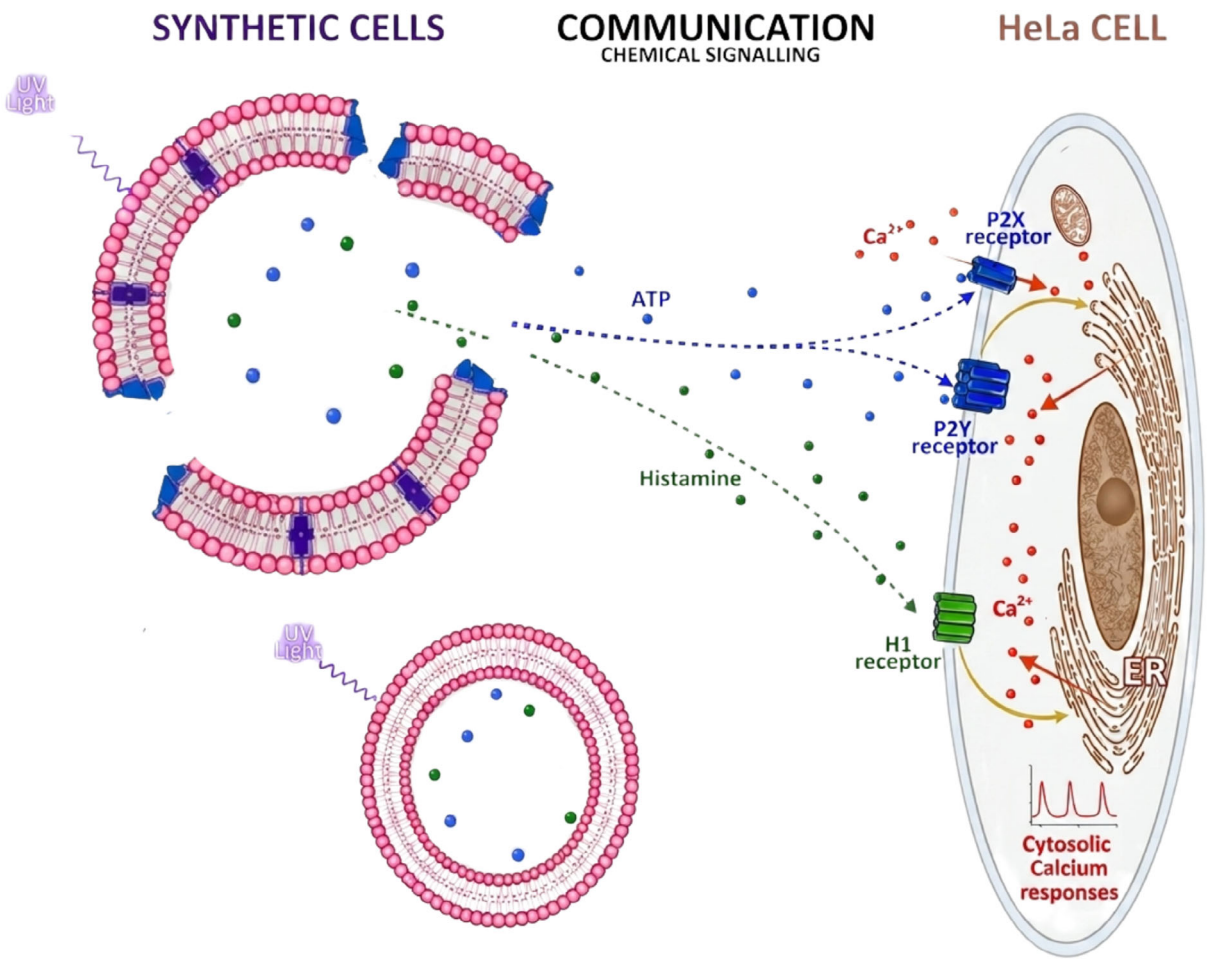

FIGURE 1 | Schematic representation of light-controlled communication between a synthetic cell and a living cell. A SC incorporating transmembrane photoresponsive azobenzene amphiphile, in purple, undergoes UV-induced $E \rightarrow Z$ photoisomerization, increasing membrane destabilization and triggering the release of encapsulated signaling molecules (ATP and histamine). These diffusible mediators activate P2Y, P2X, and H1 receptors on the target cell membrane, leading to cytosolic calcium responses including oscillatory patterns, transient spikes, and sustained plateaus. In contrast, the nonfunctionalized SC shown at the bottom remains insensitive to UV irradiation and does not release cargo molecules. Overall, this platform illustrates a biomimetic strategy for externally controlled cell–cell communication mediated by light-responsive synthetic compartments.

amine, it was subjected to diazotization by using a mixture of hydrochloric acid and sodium nitrite. The in situ formed diazonium salts were then treated with phenol to form the azobenzene derivative **4**. Following this, the phenolic –OH group on the other end of the azobenzene was alkylated using 1,6-dibromohexane to produce the bromide intermediate **5**, which was finally treated with di-Boc-protected-1,4,7-triazacyclononane (TACN) to form compound **6**. Finally, the Boc-protecting groups were removed from the TACN head group by treatment with strong acid (6 M HCl) to yield the target compound **7** (Scheme 1). The compound identity was confirmed by ^{1}H, ^{13}C NMR, and HRMS (Figures S1 and S2). The obtained spectra were fully consistent with the literature data for the target compound [28, 55].

2.3 | Compound 7-Zn Optical Characterization

Photoswitchable compound **7** was dissolved at a final concentration of 90 μM in 5 mM HEPES–KOH buffer (pH 7.6) in the presence of equimolar $ZnCl_2$. Zinc ions (Zn^{2+}) spontaneously coordinate with the nitrogen atoms in the TACN group, thus enhancing the polarity of the hydrophilic head. Absorbance measurements of compound **7**-Zn were performed at room temperature (23°C) using a 1-mL quartz cuvette with a 1-cm path length (Hellma Analytics, Germany). UV illumination was provided by a 10-W portable torch emitting at a $\lambda_{max} = 365$ nm (Alonefire SV003), while white light illumination was supplied by a white LED lamp (11 W). Samples were illuminated directly in the cuvette, and absorption spectra were recorded immediately after irradiation using an Agilent 8453 UV–Visible spectrophotometer (Agilent Technologies, Inc., Santa Clara, CA, USA). The illumination time required to induce each geometric isomerization was set to 1 min for every experiment.

2.4 | Giant Unilamellar Vesicle Preparation

Giant unilamellar vesicles were prepared using phase transfer method [56, 57] with the following modifications. The aqueous core of vesicles (40 μL) consisted of phosphate buffer solution (10 mM, pH 8), sucrose (200 mM), and, when specified, encapsulated cargo molecules (ATP 10 mM and histamine 10 mM). The

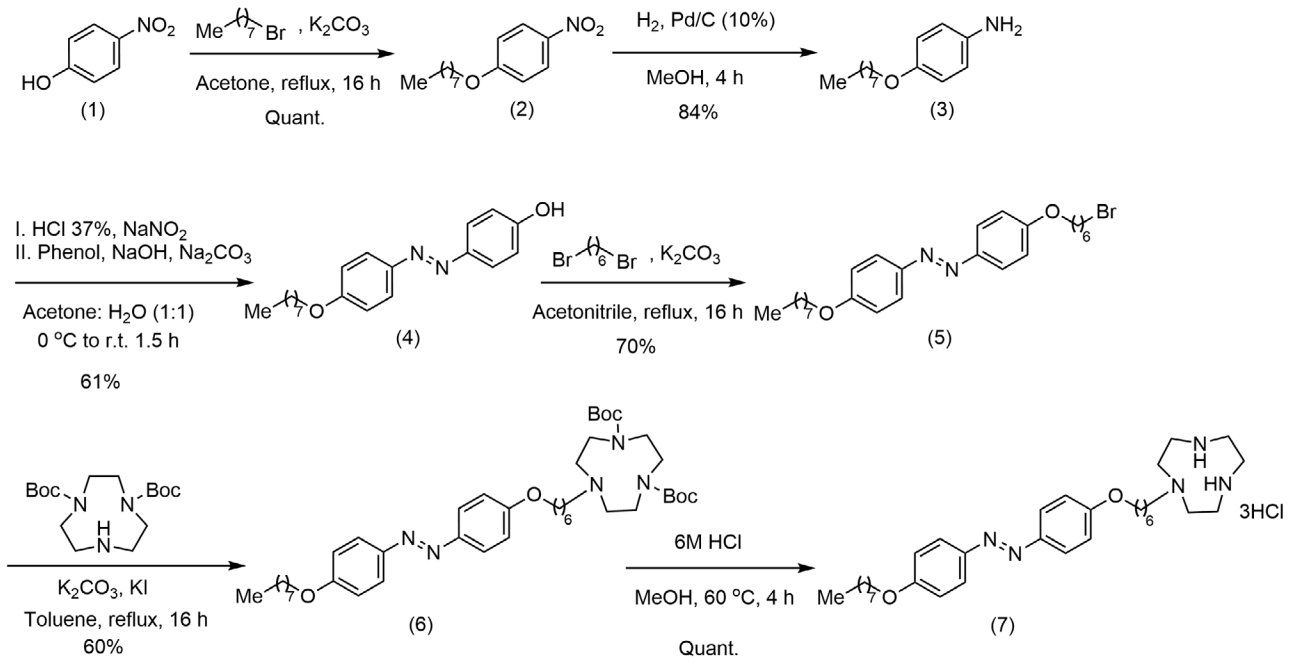

SCHEME 1 | Synthesis of photoswitchable amphiphilic compound **7**.

external aqueous phase was prepared in a final volume of 1 mL containing isotonic phosphate buffer solution (10 mM, pH 8) and glucose (200 mM). The organic phase was prepared by dispersing 0.3 mM POPC and 0.6 mM cholesterol in 1.8 mL of mineral oil (Figure S3a).

In a general procedure, 600 μL of the organic phase were carefully layered onto 1 mL of the external aqueous phase in a 15-mL centrifuge tube, generating a stable biphasic system. The mixture was left undisturbed for 10 min at room temperature to allow the spontaneous formation of a phospholipid monolayer at the water–oil interface, with hydrophobic tails oriented toward the oil phase and hydrophilic heads toward the aqueous phase (Figure S3b). In parallel, a water-in-oil emulsion was prepared by dispersing the internal aqueous phase into the remaining 1.2 mL of organic phase through repeated pipetting, yielding a stable emulsion (Figure S3c). The emulsion was then gently layered onto the biphasic system and centrifuged (20 min, 2500 × *g*, 25°C) forcing the droplets to cross the lipid-enriched water/oil interface and thereby inducing phase transfer and vesicle formation (Figure S3d,e). The resulting GUV pellet was resuspended in fresh external buffer and centrifuged again to remove nonentrapped agonist molecules. Subsequently, the pellet was collected in 100 μL from the bottom of the tube and either used immediately or stored at 4°C until further use (Figure S3f,g). When included in the formulation, compound **7**-Zn was incorporated into vesicle membrane by coincubation with preformed GUVs at a final concentration of 100 μM.

2.5 | Cell Culture

HeLa cells (provided from Sigma–Aldrich, Cat. Num.: 93021013, RRID: CVCL_0030) were cultured in Dulbecco's modified Eagle's medium (DMEM) (high glucose, with L-glutamine and sodium pyruvate, SIAL-DMEM-HPA) supplemented with 10% in volume of fetal bovine serum (ECS5000L, Euroclone) and 1% penicillin/streptomycin mix (15140122, Gibco). Regular passaging of cultures was performed twice a week in a 1:5 passaging ratio, using phosphate-buffered saline (PBS) without Ca^{2+} and Mg^{2+} (SIAL-PBS-1°) for culture washes and 0.125% trypsin–ethylenediaminetetraacetic acid (EDTA) solution (15090046, Gibco). For calcium imaging experiments, cells were seeded on poly-L-lysine-coated ø 18 mm glass coverslips at a density of 25×10^3 cells cm^{-2}.

2.6 | Fluorescence-Based Monitoring of Cytosolic Ca^{2+} Dynamics With Fura-2

To monitor intracellular calcium dynamics, cells were loaded with the fluorescent calcium sensor Fura-2-AM (ThermoFisher Scientific, Waltham, MA, USA). Briefly, a 2-μM dispersion of Fura-2-AM in serum-free culture media was vigorously homogenized by repeated pipetting and incubated with cells for 20 min at 37°C to promote Fura-2-AM internalization and de-esterification (Figure S4a). Once inside the cell, Fura-2 coordinates Ca^{2+} ions, causing characteristic changes in its spectroscopic properties (Figure S4b). Intracellular calcium variations were therefore monitored over time by ratiometric fluorescence measurements, recording emission at 510 nm upon alternating excitation at 340 and 380 nm (Figure S4c).

Coverslips were mounted into a customized perfusion chamber (inspection area: 50.24 mm^2) (Figure S5). The samples were then washed with Krebs–Ringer buffer (125 mM NaCl, 5 mM KCl, 1 mM Na_3PO_4, 1 mM $MgSO_4$, 5.5 mM glucose, 20 mM HEPES, pH 7.4, at 37°C) for 10 min to remove noninternalized Fura-2-AM. Fluorescence analysis was performed using an inverted Eclipse TE2000-U microscope (Nikon, Shinagawa, Tokyo, Japan) equipped with a 40x Plan Fluor oil immersion objective and a xenon arc lamp as illumination source. The excitation wavelengths 340/380 nm for Fura-2 excitation and for activation

of the photoisomerization of the compound **7**-Zn were selected using a DeltaRAM V random access monochromator, and the exposure timelapse, synchronized with the acquisition, was controlled by a mechanical shutter. A filter cube equipped with XF04-2, 520 ± 20 nm band-pass emission filter and with a dichroic mirror (Omega Optical, Brattleboro, VT, USA), was used to collect green fluorescence. Images were acquired using a Peltier cooled charge-coupled device camera (Coolsnap HQ camera, Photometrics, Tucson, AZ, USA). Photoactivation of compound **7** was achieved by continuous illumination at 380 nm for a maximum of 3 min before starting the acquisitions. Real-time processing of Fura-2 fluorescence ratios, control of the whole setup and image storage were performed by MetaFluor imaging software (version 7.7.3.0, Molecular Devices, San Jose, CA, USA). Experiments were performed acquiring pairs of fluorescence images (λ_{ex}340 nm/λ_{em}510 nm exposure 150 ms; λ_{ex}380 nm/λ_{em}510 nm exposure 80 ms) with a 2s frame rate. Average fluorescence intensity was recorded by drawing regions of interest (ROI) around each cell. Real-time processing of Fura-2 fluorescence ratios, control of the whole setup, and image storage were performed by MetaFluor imaging software (version 7.7.3.0, Molecular Devices, San Jose, CA, USA). Acquired data were processed and graphed using GraphPad Prism 8. Images were post-processed using Imagej [58].

3 | Results and Discussion

3.1 | Compound 7-Zn Spectroscopic Characterization

The photoswitching capability of compound **7**-Zn was evaluated by comparing absorption spectra recorded before and after UV irradiation. Consistent with previous reports on the same molecule [28, 55], UV exposure (λ_{max} = 365 nm) induces a reversible geometric isomerization from the thermodynamically stable *E* configuration to the *Z* form, while recovery of the *E* isomer occurs either through thermal relaxation or upon irradiation with blue (λ_{max} = 465 nm) or visible light (Figure 2a). The occurrence of this conformational transition is clearly reflected in the absorption spectra (Figure 2b), which allows discrimination between the two isomers. Specifically, the *E* isomer displays a characteristic absorption maximum at 345 nm, whose intensity is markedly reduced and concomitantly blueshifted upon conversion to the *Z* form.

Importantly, the isomerization process is fully reversible and reproducible up to 10 times without any detectable loss in photoswitching efficiency (Figure S6a), indicating high photostability and robustness of the switching mechanism. Moreover, by modulating the intensity of the UV irradiation while maintaining a constant exposure time, the extent of *E*-to-*Z* isomerization can be finely controlled, enabling tunable population distributions of the two isomers, as shown in Figure S6b. This behavior highlights the potential of the system for quantitative and controllable light-driven modulation.

3.2 | Light-Driven Communication Between Synthetic and HeLa Cells

A combination of canonical agonists involved in calcium-mediated signaling pathways was selected, namely ATP and histamine. ATP is capable of inducing intracellular calcium increases via both ionotropic purinergic receptors (P2X ligand-gated ion channels), which mediate calcium influx from the extracellular environment, and metabotropic G_q-protein-coupled receptors (P2Y). Histamine, through activation of H1 Gq-coupled receptors, similarly promotes intracellular calcium release. In both metabotropic pathways, receptor activation stimulates phospholipase C (PLC)-dependent production of inositol-1,4,5-trisphosphate (IP3), ultimately triggering calcium release from endoplasmic reticulum storage.

As a preliminary validation step, extracellular ATP and histamine were directly administered to HeLa cells loaded with the

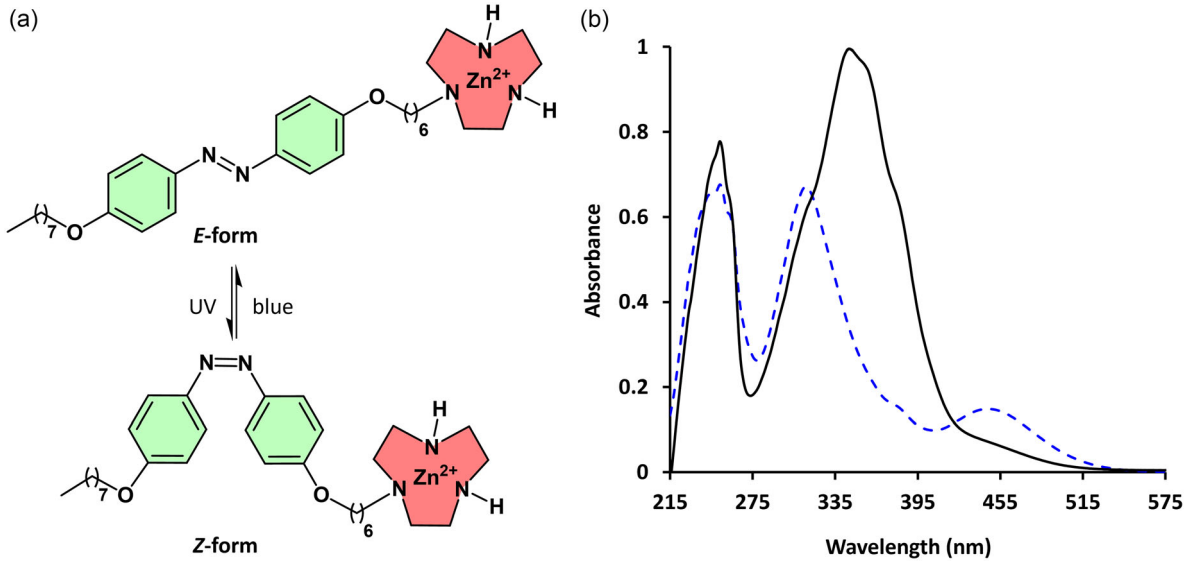

FIGURE 2 | Photoswitching behavior of compound **7**-Zn. (a) Chemical structure and geometry of the *E*- and *Z*-isomers. (b) Absorption spectra of compound **7** (90 μM) in HEPES (5 mM, pH 7.6) in the *E* (black line) and *Z* (blue dotted line) form.

cytosolic calcium indicator Fura-2 (as described in Section 2.6) to verify the characteristic calcium response generated by the selected agonists. Figure 3 shows the repetitive intracellular calcium oscillations observed upon addition of the ATP/histamine mixture (both 10 μM final concentration). Calcium-dependent fluorescence fluctuations persisted throughout the stimulation period and progressively decreased after perfusion with fresh Krebs–Ringer buffer was restored following 6 min of exposure (time interval indicated by dashed lines), eventually returning to basal levels (Figure 3c). Each trace represents the calcium response of an individual cell. The overall behavior of the analyzed field is illustrated in the animation shown in Figure S7a and in SI S1.AVI.

Subsequently, SCs were employed as vectors for the controlled and localized delivery of the two calcium-mobilizing agonists. ATP and histamine (both at 10 mM final concentration) were encapsulated within the vesicle lumen during GUV preparation. As a control, ATP/histamine-loaded SCs lacking the photoswitchable membrane component were added to HeLa cells to evaluate the possible occurrence of nonspecific cellular activation. Following the Fura-2-AM incubation procedure with cells, 100 μL of SC suspension were gently added to the adherent HeLa cells. SCs were allowed to sediment for 10 min to promote close spatial proximity between vesicles and cells. After visual confirmation of sedimentation, perfusion was resumed for an additional 5 min to remove nonsedimented SCs. Then, the field of interest was selected prior to fluorescence imaging experiments (Figure 4a). Importantly, neither the mere presence of ATP/histamine-loaded SCs adjacent to cells nor UV irradiation of these vesicles in the absence of the photoswitchable amphiphile elicited detectable calcium oscillations (Figure 4c). Bright-field imaging further confirmed that SCs lacking the photoswitchable membrane component remained structurally intact following illumination, demonstrating that UV exposure alone was insufficient to induce vesicle rupture (Figure 4b). These controls demonstrate the absence of nonspecific agonist leakage, exclude spontaneous calcium oscillations under the adopted experimental conditions, and confirm that the sole presence of agonist-loaded SCs near cells does not induce detectable cellular activation (Figure 4).

After confirming through control experiments that ATP/histamine-loaded SCs lacking the photoswitchable component did not induce

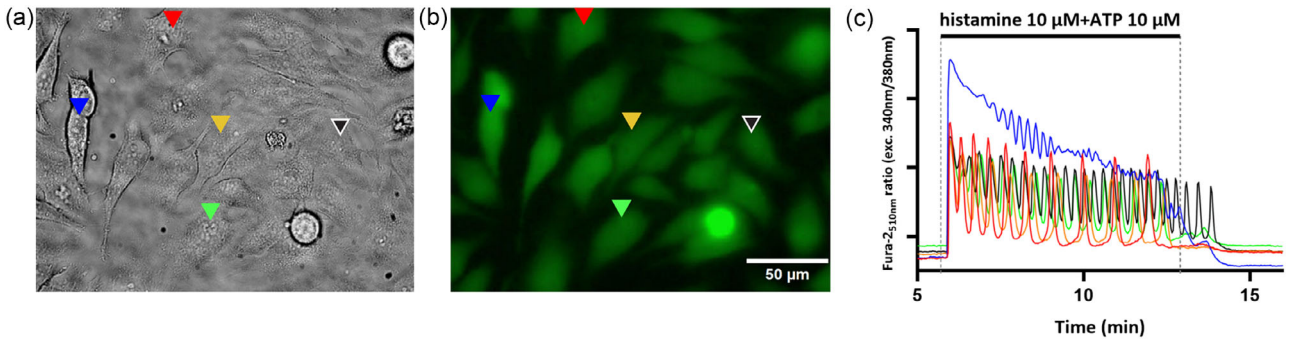

FIGURE 3 | (a) Bright field and (b) fluorescence micrographs of Fura-2-loaded HeLa cells. (c) Time-resolved traces of cytosolic calcium dynamics in HeLa cells following exposure to a mix of 10 μM histamine and 10 μM ATP. The graph shows changes of Fura-2 fluorescence ratio (ex. 340 nm/380 nm; em. 510 nm) over time. Perfusion was stopped at 5.5 min (left vertical dotted line), and the agonist mixture was added at 6 min, allowing cells to be exposed to the stimulus for 7 min. Perfusion was subsequently restored at 13 min (right vertical dotted line). Each trace represents the response of an individual cell indicated in the micrographs (a,b) by a color-matching marker.

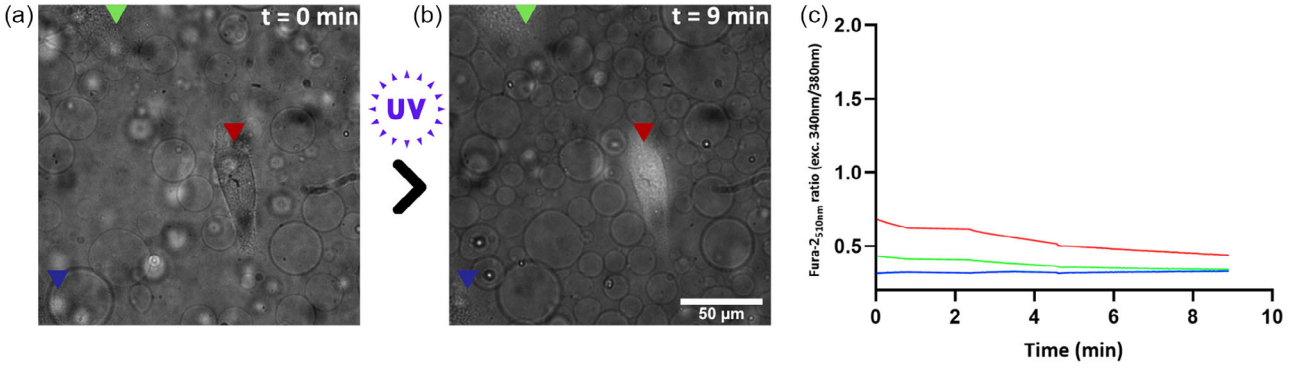

FIGURE 4 | Bright-field micrographs showing nonfunctionalized ATP/histamine-loaded SCs localized in close proximity to HeLa cells (highlighted with colored markers) before (a) and after UV illumination (b). No vesicle rupture was observed following a 3-min UV irradiation in the absence of the compound **7**. The apparent increase in SC number after illumination is attributable to delayed vesicle sedimentation during image acquisition. (c) Consistently, live-cell Fura-2 imaging (acquired approximately 10 s after the transmitted-light image in b, corresponding to $t = 0$ in c) revealed neither cytosolic calcium oscillations nor significant calcium increases related to the three selected cells, confirming the absence of nonspecific cellular responses unrelated to SC bursting and cargo release, such as passive cargo leakage or residual ATP/histamine contamination in the external suspension buffer. Each trace corresponds to the calcium response of an individual cell identified in panel (a,b) by a color-matched marker.

detectable cellular responses, the final experiment was performed on cancer HeLa cell samples using SCs functionalized with the photoswitchable amphiphile. Compound **7** at the concentration of 6 mM, was incubated for 10 min at room temperature in the dark with an equimolar solution of $ZnCl_2$. Membrane functionalization was achieved by incubating the giant vesicles with 100 μM compound **7**-Zn (193.4 μL di GUVs + 6.6 μL di **7**-Zn 3 mM) in the dark at room temperature for 10 min prior to their addition to the cellular preparation. Since compound **7** is supplied through the external vesicle aqueous phase, it is expected to interact with GUVs by partitioning into the membrane, initially at the outer leaflet. This insertion process has been previously characterized using the same postincubation protocol, which enabled systematic investigation of the influence of photoswitch concentration and UV irradiation intensity on membrane permeability [28]. Importantly, this strategy is not limited to a specific vesicle preparation method but can, in principle, be applied to virtually any preformed lipid-based compartment. In the present study, the membrane composition was adjusted to a POPC:cholesterol:amphiphile **7** ratio of 1:2:0.3, providing a cholesterol-rich environment that favors immediate bursting upon photoactivation. The resulting functionalized SCs were brought into contact with cultured cells to evaluate their performance as light-responsive cargo delivery systems. Following photo-triggered rupture of functionalized SCs (Figure 5a,b), most neighboring cells, identified by the colored markers in Figure 5c, displayed the expected oscillatory cytosolic calcium transients (Figure 5d), indicating successful exposure to the released signaling molecules. Calcium oscillations persisted for several minutes following SC disruption and closely resembled the calcium dynamics observed during direct extracellular stimulation with agonists.

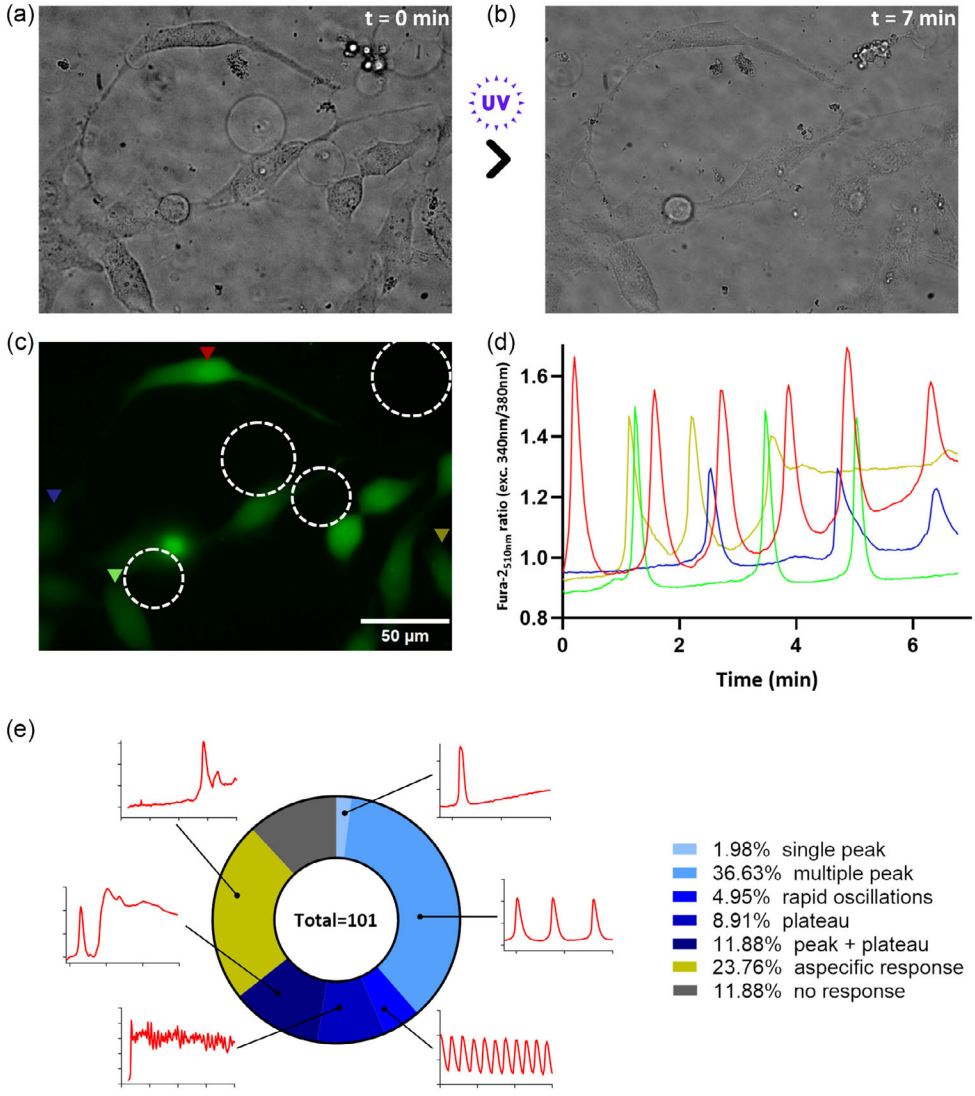

FIGURE 5 | Light-triggered communication between synthetic and HeLa cells. Top panels: bright-field micrographs acquired before 380 nm illumination, showing SCs localized in close proximity to HeLa cells (a), and after UV-induced SC rupture (b). Fluorescence micrograph of Fura-2-loaded HeLa cells (c) exposed to the localized release of ATP and histamine following SC bursting (SCs are not visible in fluorescence mode and are indicated by dashed white circles). Release of ATP and histamine induces characteristic cytosolic calcium oscillations, shown in panel (d) as time-dependent variations of the Fura-2 fluorescence ratio (excitation 340/380 nm, emission 510 nm). Each trace corresponds to the calcium response of an individual cell identified in Panel (c) by a color-matched marker. (e) Pie chart summarizing the distribution of the different cellular response profiles. Representative calcium traces for each response type are shown as red curves and linked to the corresponding section of the chart. Percentages are calculated over the total number of analyzed cells (101 cells from eight independent replicates).

These findings demonstrate that localized release of signal molecules from SCs is sufficient to reproduce physiological calcium signaling responses comparable to conventional bulk stimulation. Although prolonged UV exposure is known to induce cellular stress and perturb calcium homeostasis, the short irradiation time required to trigger SC rupture (<1 min) did not produce detectable adverse effects within the experimental timeframe (<10 min), as evidenced by the preserved morphology and responsiveness of the cells. Calcium response analysis was performed on 101 individual cells collected from eight independent coverslips ($n = 8$). Different response profiles were identified following stimulation. Specifically, 36.63% of cells exhibited repeated discrete calcium peaks, while 11.88% displayed an initial isolated peak followed by a sustained plateau phase. A further 8.91% of cells reached a plateau often accompanied by smaller oscillatory events, whereas 4.95% showed rapid calcium oscillations and 1.98% displayed a single-peak like response. In addition, 23.76% of cells showed aspecific response, typically characterized by delayed calcium peaks potentially arising from paracrine intercellular communication or from vesicle rupture occurring outside the field of view. These events were therefore excluded from the category of specific responses, which overall accounted for 64.36% of the analyzed cells. Only 11.88% of cells did not exhibit any detectable response to stimulation (Figure 5e). The overall behavior of the analyzed field is illustrated in the animation shown in Figure S7b and in SI S2.AVI.

Overall, these results strongly support the use of SCs as platforms for controlled and spatially localized cargo delivery. Calcium imaging experiments demonstrate that mammalian cells are capable of responding reproducibly to agonists released from nearby synthetic compartments, producing signaling dynamics analogous to those induced by direct extracellular administration. Notably, effective stimulation required substantially higher cargo concentrations within the SC lumen compared to conventional bulk assays (1000-fold higher for both ATP and histamine), likely to compensate for dilution effects arising from diffusion into the extracellular environment following release. Nevertheless, these concentrations were sufficient to elicit robust physiological cellular responses, highlighting the feasibility and effectiveness of the proposed strategy for localized chemical communication between synthetic and living cells.

The selected experimental setup was designed to maximize biomimicry and biocompatibility while avoiding the use of potentially cytotoxic monomers commonly employed in polymer-based artificial cell architectures [25, 27]. Instead, we employed a membrane-forming photoswitchable amphiphile capable of efficiently incorporating into preformed phospholipid GUVs. Previous studies have reported minimal or no cytotoxicity for cationic amphiphiles structurally related to amphiphile **7** [59, 60] as well as for photolipid-based vesicular systems [61]. In addition, the TACN headgroup of compound **7** exhibits negligible cytotoxicity at concentrations up to 250 μM [62]. In our approach, amphiphile **7** is administered to pre-existing membrane-bound compartments immediately prior to their introduction into cell cultures. This decouples membrane functionalization from vesicle preparation and more closely resembles a realistic delivery scenario. Although the biomedical use of synthetic photoswitches remains at an early stage, their functionality has already been demonstrated in both cellular and animal models [63]. Likewise, POPC-based vesicles are widely regarded as biocompatible carrier for controlled cargo delivery [64–66].

A current limitation of the platform is the requirement for UV-light activation, which presently confines potential applications to settings where localized illumination is feasible, such as topical [13] and ocular [14] therapies. Nevertheless, the incorporation of visible- or near-infrared-responsive photoswitches [67, 68] could substantially broaden the therapeutic scope of this approach, including light-activated radio- and chemotherapy [69].

4 | Conclusions

In this work, a light-responsive SC platform capable of establishing chemically mediated communication with mammalian cells through the controlled release of signaling molecules has been developed. By incorporating a photoswitchable azobenzene-based amphiphile into giant unilamellar vesicle membranes, synthetic compartments whose permeability and stability can be remotely regulated by optical stimulation were engineered. Upon UV irradiation, photoinduced membrane destabilization triggered vesicle rupture and release of encapsulated cargo molecules. Spectroscopic characterization demonstrated the robust and reversible photoswitching behavior of amphiphilic Compound **7**, while microscopy experiments provided functional evidence of its successful incorporation into SC membranes. Specifically, only functionalized SCs underwent light-triggered membrane destabilization and subsequent cargo release upon UV irradiation whereas SCs lacking Compound **7** remained structurally stable under UV exposure.

Using ATP and histamine as model signaling molecules, cargo release from SCs positioned near HeLa cells was shown to induce reproducible intracellular calcium responses, including oscillatory calcium transients closely resembling those observed upon conventional extracellular stimulation. Control experiments demonstrated that neither UV irradiation alone nor rupture of empty vesicles elicited significant calcium activity, confirming that the observed signaling responses originated specifically from the released agonists.

These findings demonstrate that SCs can function as remotely activated chemical messengers capable of transmitting biologically relevant information to mammalian cells. Although effective stimulation required relatively high encapsulated cargo concentrations to compensate for diffusion-driven dilution following release, robust physiological responses were nonetheless observed, highlighting the feasibility of localized signaling mediated by synthetic compartments.

Beyond its relevance for investigating minimal stimulus–response systems and bio-hybrid communication networks, the proposed strategy opens interesting biotechnological perspectives. Light-responsive SCs may serve as programmable platforms for targeted drug delivery, localized therapeutic stimulation, or spatiotemporally controlled modulation of cellular behavior. Future developments could involve the implementation of visible- or near-infrared-responsive photoswitches to improve biocompatibility, the integration of more sophisticated biochemical reaction

networks, and the introduction of autonomous sensing and processing capabilities. In the longer term, such systems may contribute to the development of advanced synthetic-biological interfaces for precision medicine, tissue engineering, and externally controllable therapeutic technologies.

Acknowledgments

This research was supported by the European Union–NextGenerationEU, Mission 4, Component 2, Investment 1.1, under PRIN 2022 (CUP H53D23003920006 and CUP B53D23013870006), and PRIN 2022 PNRR (CUP H53D23007520001). Authors from the University of Siena acknowledge financial support under the National Recovery and Resilience Plan (PNRR), Mission 4, Component 2, Investment 1.4, funded by the European Union – NextGenerationEU – Project PNRR CN3 "mRNA" – Spoke 5 – CUP B63C22000610006, and Investment 1.5 – Creation and reinforcement of an "innovation ecosystem,", construction of "leader territoriali R&S" – Project THE (Tuscan Health Ecosystem) – Spoke 4 – Nanotechnologies for diagnosis and therapy – project code ECS00000017, CUP B63C22000680007 and by the Marie Skłodowska-Curie Doctoral Network ComeInCell, funded by the European Union's Horizon Europe research and innovation programme under the grant agreement no. 101168939.

Open access publishing facilitated by Universita degli Studi di Bari Aldo Moro, as part of the Wiley - CRUI-CARE agreement.

Funding

This work was supported by the European Union–NextGenerationEU, Mission 4, Component 2, Investment 1.1, under PRIN 2022 (CUP H53D23003920006 and CUP B53D23013870006), PRIN 2022 PNRR (CUP H53D23007520001), Mission 4, Component 2, Investment 1.4, funded by the European Union – NextGenerationEU – Project PNRR CN3 "mRNA" – Spoke 5 (CUP B63C22000610006), Investment 1.5 – Creation and reinforcement of an "innovation ecosystem," construction of "leader territoriali R&S" – Project THE (Tuscan Health Ecosystem) – Spoke 4 – Nanotechnologies for diagnosis and therapy – Project Code ECS00000017 (CUP B63C22000680007), and Marie Skłodowska-Curie Doctoral Network ComeInCell, funded by the European Union's Horizon Europe research and innovation programme (Grant Agreement No. 101168939).

Conflicts of Interest

The authors declare no conflicts of interest.

Data Availability Statement

The data supporting the findings of this study are available within the article and its supporting information file.

References

1. C. Guindani, L. C. da Silva, S. Cao, T. Ivanov, and K. Landfester, "Synthetic Cells: From Simple Bio-Inspired Modules to Sophisticated Integrated Systems," *Angewandte Chemie* 134 (2022): e202110855, https://doi.org/10.1002/ange.202110855.

2. V. Noireaux, Y. T. Maeda, and A. Libchaber, "Development of an Artificial Cell, from Self-Organization to Computation and Self-Reproduction," *Proceedings of the National Academy of Sciences* 108 (2011): 3473–3480, https://doi.org/10.1073/pnas.1017075108.

3. J. C. Blain and J. W. Szostak, "Progress Toward Synthetic Cells," *Annual Review of Biochemistry* 83 (2014): 615–640, https://doi.org/10.1146/annurev-biochem-080411-124036.

4. A. Salehi-Reyhani, O. Ces, and Y. Elani, "Artificial Cell Mimics as Simplified Models for the Study of Cell Biology," *Experimental Biology and Medicine* 242 (2017): 1309–1317, https://doi.org/10.1177/1535370217711441.

5. E. Altamura, P. Albanese, F. Mavelli, and P. Stano, "The Rise of the Nested Multicompartment Model in Synthetic Cell Research," *Frontiers in Molecular Biosciences* 8 (2021): 750576, https://doi.org/10.3389/fmolb.2021.750576.

6. W. Sato, T. Zajkowski, F. Moser, and K. P. Adamala, "Synthetic Cells in Biomedical Applications," *WIREs Nanomedicine and Nanobiotechnology* 14 (2022): e1761, https://doi.org/10.1002/wnan.1761.

7. M. A. Boyd and N. P. Kamat, "Designing Artificial Cells towards a New Generation of Biosensors," *Trends in Biotechnology* 39 (2021): 927–939, https://doi.org/10.1016/j.tibtech.2020.12.002.

8. I. Gispert, J. W. Hindley, C. P. Pilkington, et al., "Stimuli-Responsive Vesicles as Distributed Artificial Organelles for Bacterial Activation," *Proceedings of the National Academy of Sciences* 119 (2022): e2206563119, https://doi.org/10.1073/pnas.2206563119.

9. K. P. Adamala, D. A. Martin-Alarcon, K. R. Guthrie-Honea, and E. S. Boyden, "Engineering Genetic Circuit Interactions Within and Between Synthetic Minimal Cells," *Nature Chemistry* 9 (2017): 431–439, https://doi.org/10.1038/nchem.2644.

10. E. Altamura, F. Milano, R. R. Tangorra, et al., "Highly Oriented Photosynthetic Reaction Centers Generate a Proton Gradient in Synthetic Protocells," *Proceedings of the National Academy of Sciences* 114 (2017): 3837–3842, https://doi.org/10.1073/pnas.1617593114.

11. E. Altamura, P. Albanese, R. Marotta, et al., "Chromatophores Efficiently Promote Light-Driven ATP Synthesis and DNA Transcription Inside Hybrid Multicompartment Artificial Cells," *Proceedings of the National Academy of Sciences* 118 (2021): e2012170118, https://doi.org/10.1073/pnas.2012170118.

12. N. Krinsky, M. Kaduri, A. Zinger, et al., "Synthetic Cells Synthesize Therapeutic Proteins inside Tumors," *Advanced Healthcare Materials* 7 (2018): 1701163, https://doi.org/10.1002/adhm.201701163.

13. A. Yaghmur, L. Paasonen, M. Yliperttula, A. Urtti, and M. Rappolt, "Structural Elucidation of Light Activated Vesicles," *Journal of Physical Chemistry Letters* 1 (2010): 962–966, https://doi.org/10.1021/jz100226v.

14. H. A. M. Abdelmohsen, N. A. Copeland, and J. G. Hardy, "Light-Responsive Biomaterials for Ocular Drug Delivery," *Drug Delivery and Translational Research* 13 (2023): 2159–2182, https://doi.org/10.1007/s13346-022-01196-5.

15. G. Rampioni, F. D'Angelo, L. Leoni, and P. Stano, "Gene-Expressing Liposomes as Synthetic Cells for Molecular Communication Studies," *Frontiers in Bioengineering and Biotechnology* 7 (2019): 1, https://doi.org/10.3389/fbioe.2019.00001.

16. K. Ikari, Y. Sakuma, T. Jimbo, et al., "Dynamics of Fatty Acid Vesicles in Response to pH Stimuli," *Soft Matter* 11 (2015): 6327–6334, https://doi.org/10.1039/C5SM01248A.

17. Y. Miele, Z. Medveczky, G. Holló, et al., "Self-Division of Giant Vesicles Driven by an Internal Enzymatic Reaction," *Chemical Science* 11 (2020): 3228–3235, https://doi.org/10.1039/C9SC05195C.

18. G. Holló, Y. Miele, F. Rossi, and I. Lagzi, "Shape Changes and Budding of Giant Vesicles Induced by an Internal Chemical Trigger: An Interplay Between Osmosis and pH Change," *Physical Chemistry Chemical Physics* 23 (2021): 4262–4270, https://doi.org/10.1039/D0CP05952H.

19. Y. Miele, S. J. Jones, F. Rossi, P. A. Beales, and A. F. Taylor, "Collective Behavior of Urease pH Clocks in Nano- and Microvesicles Controlled by Fast Ammonia Transport," *The Journal of Physical Chemistry Letters* 13 (2022): 1979–1984, https://doi.org/10.1021/acs.jpclett.2c00069.

20. C. Vanhille-Campos and A. Šarić, "Modelling the Dynamics of Vesicle Reshaping and Scission under Osmotic Shocks," *Soft Matter* 17 (2021): 3798–3806, https://doi.org/10.1039/D0SM02012E.

21. M. Kurisu, H. Aoki, T. Jimbo, et al., "Reproduction of Vesicles Coupled with a Vesicle Surface-Confined Enzymatic Polymerisation," *Communications Chemistry* 2 (2019): 117, https://doi.org/10.1038/s42004-019-0218-0.

22. K. Kurihara, M. Tamura, K.-I. Shohda, T. Toyota, K. Suzuki, and T. Sugawara, "Self-Reproduction of Supramolecular Giant Vesicles Combined with the Amplification of Encapsulated DNA," *Nature Chemistry* 3 (2011): 775–781, https://doi.org/10.1038/nchem.1127.

23. M. Dwidar, Y. Seike, S. Kobori, C. Whitaker, T. Matsuura, and Y. Yokobayashi, "Programmable Artificial Cells Using Histamine-Responsive Synthetic Riboswitch," *Journal of the American Chemical Society* 141 (2019): 11103–11114, https://doi.org/10.1021/jacs.9b03300.

24. F. Rossi, S. Ristori, and A. Abou-Hassan, "Multiscale Approach for Tuning Communication among Chemical Oscillators Confined in Biomimetic Microcompartments," *Accounts of Chemical Research* 57 (2024): 2607–2619, https://doi.org/10.1021/acs.accounts.4c00232.

25. S. Sethi, C. Sharma, and A. Walther, "ATP-Powered Signaling Between Artificial and Living Cells," *Angewandte Chemie International Edition* 64 (2025): e202517843, https://doi.org/10.1002/anie.202517843.

26. M. E. Allen, S. Frank, M. Louis, A. Saha, A. Heidari, and S. V. Wegner, "Let There Be Light! Light as an Engine and Regulator in Synthetic Cells," *Angewandte Chemie International Edition* 65 (2026): e4174230, https://doi.org/10.1002/anie.4174230.

27. A. B. Cook, S. Sun, Y. Li, J. Scheerstra, and J. C. M. van Hest, "Photoactivatable Synthetic Exosomes for RNA-Based Communication Between Artificial Cells and Living Cells," *Angewandte Chemie International Edition* 64 (2025): e202514041, https://doi.org/10.1002/anie.202514041.

28. P. Albanese, S. Cataldini, C. Z.-J. Ren, et al., "Light-Switchable Membrane Permeability in Giant Unilamellar Vesicles," *Pharmaceutics* 14 (2022): 2777, https://doi.org/10.3390/pharmaceutics14122777.

29. P. Albanese, S. Cataldini, S. Amoroso, et al., "Photomodulation of Vesicle Dynamics Using Fluorescent Photoswitchable Amphiphiles," *Journal of Materials Chemistry B* 14 (2026): 3093–3108, https://doi.org/10.1039/D5TB01894C.

30. N. Abdollahi, D. Messmer, V. Mihali, and C. G. Palivan, "Magnetically Controlled Polymer Giant Unilamellar Vesicles," *Small* 21 (2025): 2502552, https://doi.org/10.1002/smll.202502552.

31. K. Karamdad, J W. Hindley, G. Bolognesi, et al., "Engineering Thermoresponsive Phase Separated Vesicles Formed *via* Emulsion Phase Transfer as a Content-Release Platform," *Chemical Science* 9 (2018): 4851–4858, https://doi.org/10.1039/C7SC04309K.

32. W. N. Bahutair, W. H. Abuwatfa, and G. A. Husseini, "Ultrasound Triggering of Liposomal Nanodrugs for Cancer Therapy A Review," *Nanomaterials* 12 (2022): 3051, https://doi.org/10.3390/nano12173051.

33. M. Löffler, D. Repp, F. Beka, and R. Wieneke, "Photoswitchable Detergents for Light-Controlled Liposome Lysis and Channel Gating," *ChemBioChem* 25 (2024): e202400517, https://doi.org/10.1002/cbic.202400517.

34. Y. Noguchi, S. Sasaki, Y. Liao, M. Matsuo, K. Asakura, and T. Banno, "Photoinduced Shape Changes of Giant Vesicles Comprising Phospholipids and Azobenzene-Containing Cationic Amphiphiles," *Chemistry – An Asian Journal* 20 (2025): e202401426, https://doi.org/10.1002/asia.202401426.

35. A. Diguet, M. Yanagisawa, Y.-J. Liu, et al., "UV-Induced Bursting of Cell-Sized Multicomponent Lipid Vesicles in a Photosensitive Surfactant Solution," *Journal of the American Chemical Society* 134 (2012): 4898–4904, https://doi.org/10.1021/ja211664f.

36. T. Hamada, R. Sugimoto, T. Nagasaki, and M. Takagi, "Photochemical Control of Membrane Raft Organization," *Soft Matter* 7 (2011): 220–224, https://doi.org/10.1039/C0SM00797H.

37. M. Aleksanyan, A. Grafmüller, F. Crea, et al., "Photomanipulation of Minimal Synthetic Cells: Area Increase, Softening, and Interleaflet Coupling of Membrane Models Doped with Azobenzene-Lipid Photoswitches," *Advanced Science* 10 (2023): 2304336, https://doi.org/10.1002/advs.202304336.

38. K. A. Alberto, M. N. Hasna Begam, H. Xiong, et al., "Fully Atomistic Molecular Dynamics Modeling of Photoswitchable Azo-PC Lipid Bilayers: Structure, Mechanical Properties, and Drug Permeation," *Nanoscale* 17 (2025): 2032–2042, https://doi.org/10.1039/D4NR02509A.

39. A. Mangiarotti, M. Aleksanyan, M. Siri, T.-W. Sun, R. Lipowsky, and R. Dimova, "Photoswitchable Endocytosis of Biomolecular Condensates in Giant Vesicles," *Advanced Science* 11 (2024): 2309864, https://doi.org/10.1002/advs.202309864.

40. S. D. Pritzl, J. Morstein, S. Kahler, D. B. Konrad, D. Trauner, and T. Lohmüller, "Postsynthetic Photocontrol of Giant Liposomes via Fusion-Based Photolipid Doping," *Langmuir* 38 (2022): 11941–11949, https://doi.org/10.1021/acs.langmuir.2c01685.

41. S. D. Pritzl, P. Urban, A. Prasselsperger, et al., "Photolipid Bilayer Permeability Is Controlled by Transient Pore Formation," *Langmuir* 36 (2020): 13509–13515, https://doi.org/10.1021/acs.langmuir.0c02229.

42. C. Pernpeintner, J. A. Frank, P. Urban, et al., "Light-Controlled Membrane Mechanics and Shape Transitions of Photoswitchable Lipid Vesicles," *Langmuir* 33 (2017): 4083–4089, https://doi.org/10.1021/acs.langmuir.7b01020.

43. P. Urban, S. D. Pritzl, D. B. Konrad, et al., "Light-Controlled Lipid Interaction and Membrane Organization in Photolipid Bilayer Vesicles," *Langmuir* 34 (2018): 13368–13374, https://doi.org/10.1021/acs.langmuir.8b03241.

44. P. Urban, S. D. Pritzl, M. F. Ober, et al., "A Lipid Photoswitch Controls Fluidity in Supported Bilayer Membranes," *Langmuir* 36 (2020): 2629–2634, https://doi.org/10.1021/acs.langmuir.9b02942.

45. M. Doroudgar, J. Morstein, J. Becker-Baldus, D. Trauner, and C. Glaubitz, "How Photoswitchable Lipids Affect the Order and Dynamics of Lipid Bilayers and Embedded Proteins," *Journal of the American Chemical Society* 143 (2021): 9515–9528, https://doi.org/10.1021/jacs.1c03524.

46. S. Moffa, S. Pilato, M. Ciulla, et al., "Recent Advances in Stimuli-Responsive Membranes: From Supramolecular Design to Controlled Permeability," *Membranes* 16 (2026): 89, https://doi.org/10.3390/membranes16030089.

47. Y. Qutbuddin, A. Guinart, S. Gavrilović, K. Al Nahas, B. L. Feringa, and P. Schwille, "Light-Activated Synthetic Rotary Motors in Lipid Membranes Induce Shape Changes Through Membrane Expansion," *Advanced Materials* 36 (2024): 2311176, https://doi.org/10.1002/adma.202311176.

48. V. N. Georgiev, A. Grafmüller, D. Bléger, et al., "Area Increase and Budding in Giant Vesicles Triggered by Light: Behind the Scene," *Advanced Science* 5 (2018): 1800432, https://doi.org/10.1002/advs.201800432.

49. S. Moffa, S. Carradori, F. Melfi, et al., "Fine-Tuning of Membrane Permeability by Reversible Photoisomerization of Aryl-Azo Derivatives of Thymol Embedded in Lipid Nanoparticles," *Colloids and Surfaces B: Biointerfaces* 241 (2024): 114043, https://doi.org/10.1016/j.colsurfb.2024.114043.

50. P. M. Gardner, K. Winzer, and B. G. Davis, "Sugar Synthesis in a Protocellular Model Leads to a Cell Signalling Response in Bacteria," *Nature Chemistry* 1 (2009): 377–383, https://doi.org/10.1038/nchem.296.

51. R. Lentini, S. P. Santero, F. Chizzolini, et al., "Integrating Artificial with Natural Cells to Translate Chemical Messages that Direct *E. Coli* Behaviour," *Nature Communications* 5 (2014): 4012, https://doi.org/10.1038/ncomms5012.

52. Ö. D. Toparlak, J. Zasso, S. Bridi, et al., "Artificial Cells Drive Neural Differentiation," *Science Advances* 6 (2020): eabb4920, https://doi.org/10.1126/sciadv.abb4920.

53. M. D. Bootman, K. W. Young, J. M. Young, R. B. Moreton, and M. J. Berridge, "Extracellular Calcium Concentration Controls the Frequency of Intracellular Calcium Spiking Independently of Inositol 1,4,5-Trisphosphate Production in HeLa Cells," *Biochemical Journal* 314 (1996): 347–354, https://doi.org/10.1042/bj3140347.

54. A. Okuda, K. Furuya, and T. Kiyohara, "ATP-Induced Calcium Oscillations and Change of P2Y Subtypes with Culture Conditions in HeLa Cells," *Cell Biochemistry and Function* 21 (2003): 61–68, https://doi.org/10.1002/cbf.992.

55. C. Z.-J. Ren, P. Solís Muñana, J. Dupont, S. S. Zhou, and J. L.-Y. Chen, "Reversible Formation of a Light-Responsive Catalyst by Utilizing Intermolecular Cooperative Effects," *Angewandte Chemie International Edition* 58 (2019): 15254–15258, https://doi.org/10.1002/anie.201907078.

56. S. Pautot, B. J. Frisken, and D. A. Weitz, "Production of Unilamellar Vesicles Using an Inverted Emulsion," *Langmuir* 19 (2003): 2870–2879, https://doi.org/10.1021/la026100v.

57. V. Noireaux and A. Libchaber, "A Vesicle Bioreactor as a Step toward an Artificial Cell Assembly," *Proceedings of the National Academy of Sciences* 101 (2004): 17669–17674, https://doi.org/10.1073/pnas.0408236101.

58. C. A. Schneider, W. S. Rasband, and K. W. Eliceiri, "NIH Image to ImageJ: 25 Years of Image Analysis," *Nature Methods* 9 (2012): 671–675, https://doi.org/10.1038/nmeth.2089.

59. S. Geng, Y. Wang, L. Wang, et al., "A Light-Responsive Self-Assembly Formed by a Cationic Azobenzene Derivative and SDS as a Drug Delivery System," *Scientific Reports* 7 (2017): 39202, https://doi.org/10.1038/srep39202.

60. Y. Kim, D. Jeong, V. V. Shinde, Y. Hu, C. Kim, and S. Jung, "Azobenzene-Grafted Carboxymethyl Cellulose Hydrogels with Photo-Switchable, Reduction-Responsive and Self-Healing Properties for a Controlled Drug Release System," *International Journal of Biological Macromolecules* 163 (2020): 824–832, https://doi.org/10.1016/j.ijbiomac.2020.07.071.

61. H. Xiong, K. A. Alberto, J. Youn, et al., "Optical Control of Neuronal Activities with Photoswitchable Nanovesicles," *Nano Research* 16 (2023): 1033–1041, https://doi.org/10.1007/s12274-022-4853-x.

62. S. Mcoyi, D. G. Amoako, A. M. Somboro, H. M. Khumalo, and R. B. Khan, "The Molecular Effect of 1,4,7-Triazacyclononane on Oxidative Stress Parameters in Human Hepatocellular Carcinoma (HepG2) Cells," *Journal of Biochemical and Molecular Toxicology* 34 (2020): e22607, https://doi.org/10.1002/jbt.22607.

63. K. Hüll, J. Morstein, and D. Trauner, "In Vivo Photopharmacology," *Chemical Reviews* 118 (2018): 10710–10747, https://doi.org/10.1021/acs.chemrev.8b00037.

64. G. Pabst, N. Kucerka, M. P. Nieh, and J. Katsaras, eds., *Liposomes, Lipid Bilayers and Model Membranes: From Basic Research to Application* (CRC Press, 2014), https://doi.org/10.1201/b16617.

65. D. Petroni, C. Riccardi, D. Cavasso, et al., "Synthesis and Characterization of Multifunctional Nanovesicles Composed of POPC Lipid Molecules for Nuclear Imaging," *Molecules* 26 (2021): 6591, https://doi.org/10.3390/molecules26216591.

66. E. Sánchez-López, A. Paús, I. Pérez-Pomeda, A. Calpena, I. Haro, and M. J. Gómara, "Lipid Vesicles Loaded with an HIV-1 Fusion Inhibitor Peptide as a Potential Microbicide," *Pharmaceutics* 12 (2020): 502, https://doi.org/10.3390/pharmaceutics12060502.

67. Z. Zhang, W. Wang, M. O'Hagan, J. Dai, J. Zhang, and H. Tian, "Stepping Out of the Blue: From Visible to Near-IR Triggered Photoswitches," *Angewandte Chemie International Edition* 61 (2022): e202205758, https://doi.org/10.1002/anie.202205758.

68. S. Thumser, L. Köttner, N. Hoffmann, P. Mayer, and H. Dube, "All-Red-Light Photoswitching of Indirubin Controlled by Supramolecular Interactions," *Journal of the American Chemical Society* 143 (2021): 18251–18260, https://doi.org/10.1021/jacs.1c08206.

69. P. Dunkel and J. Ilaš, "Targeted Cancer Therapy Using Compounds Activated by Light," *Cancers* 13 (2021): 3237, https://doi.org/10.3390/cancers13133237.

Supporting Information

Additional supporting information can be found online in the Supporting Information section.